Subsideband generation and modulational instability lasing in a fiber soliton laser

D. Y. Tang and S. Fleming

Optical Fiber Technology Center, The University of Sydney, Sydney, New South Wales 1430, Australia

W. S. Man, H. Y. Tam, and M. S. Demokan

Department of Electrical Engineering, The Hong Kong Polytechnic University, Hung Hom, Kowloon, Hong Kong

Received June 12, 2000; revised manuscript received December 1, 2000

We experimentally observed two forms of subsideband generation in the soliton spectrum of a passively mode-locked fiber soliton ring laser. We found that the different forms of subsideband generation are related to the different strengths of the saturable absorption in the laser cavity. Analyzing featuring of the subsideband generations, we show that they are both modulational-instability lasings of the dispersive waves in the laser.

OCIS codes: 140.7090, 140.4050, 140.3560, 060.5530, 190.3100.

1. INTRODUCTION

Sideband generation is a well-known phenomenon in ultrashort-pulse fiber soliton lasers and has been intensively investigated.[1–8] Sideband generation is referred to as the effect in a fiber soliton laser whose soliton spectrum is characterized by the appearance of sharp, well-defined discrete spectral components. Although sideband generation was initially suggested as a result of modulational instability,[1] it was found that it is in fact a result of constructive interference between dispersive waves shed by the soliton pulses circulating in the laser cavity. In a fiber soliton laser, when a soliton pulse circulates in the cavity, it periodically experiences perturbations caused by the laser gain, the output, and the nonlinear amplitude modulations. These periodic perturbations introduce resonance between dispersive waves shed by the soliton and cause redistribution of dispersive wave energy in the frequency domain.[4–7]

In this paper we report on experimental observations of subsideband generation in an ultrashort-pulse fiber soliton laser. We demonstrate experimentally that when the strength of a sideband formed by the effect mentioned above becomes strong enough, it generates itself discrete spectral components in the soliton spectrum. Phenomenologically, we call this subsideband generation. Two forms of subsideband generation, one with relatively large wavelength shifts to the unstable sideband (in the range of several nanometers), another with small wavelength shifts (less than 1 nm), are observed. We have studied mechanisms of these two forms of subsideband generation and found that they are related to the different strengths of saturable absorption in the laser cavity. Analyzing features of these two forms of subsideband generation, we further show that they are both modulational-instability lasings in the laser.

2. EXPERIMENTAL OBSERVATIONS

Our experiment is conducted on a passively mode-locked fiber soliton ring laser. Details of the laser configuration are reported in Ref. 9. Briefly, the laser cavity is ~10 m long and includes a 4-m-long 2000-ppm (parts in 10^6) erbium-doped fiber with a group-velocity dispersion of approximately (−10 ps/nm)km and two pieces of 3-m-long single-mode dispersion-shifted fiber, whose group-velocity dispersion is (−2 ps/nm)km. The nonlinear polarization-rotation technique[10,11] is used to achieve self-started mode locking in the laser. To this end, a polarization-dependent isolator together with two polarization controllers, one consisting of two quarter-wave plates and the other of two quarter-wave plates and one half-wave plate, is used to adjust the polarization of light in the cavity. The polarization-dependent isolator and the polarization controllers are mounted on a 7-cm-long fiber bench, with which accurate polarization adjustments can be easily obtained. The laser is pumped by a pigtailed InGaAsP semiconductor diode of wavelength 1480 nm. The pump laser power can be continuously adjusted. The output of the laser is taken by a 10% fiber coupler and analyzed with an optical spectrum analyzer and a commercial optical autocorrelator.

Soliton operation of the laser is obtained simply by increasing the pump power to the mode-locking threshold, which for our laser is ~100 mW. However, a soliton operation state of the laser that this increase obtained contains multiple soliton pulses in the laser cavity, and generally solitons are bunched together.[1–3] Strong interaction between the soliton pulses exists, which complicates the spectrum of the soliton pulses. To avoid the complication caused by soliton interaction, we always conducted our experiments under the condition that no interaction between solitons exists. Experimentally this is

done by carefully adjusting the laser parameters so that solitons are well separated.

A typical soliton spectrum of the laser without subsideband generation is shown in Fig. 1(a). The soliton spectrum is typical of those also observed in other fiber soliton lasers.[1–3] Sidebands caused by the periodic perturbations are clear to see. We note that the strengths of the sidebands shown in Fig. 1(a) are very asymmetric, which is a result of linear cavity-loss dispersion of the laser.[12] The sidebands have well-defined positions in the soliton spectrum, which are known to be determined by the cavity length and dispersion.[4–7] However, in contrast to the positions of sidebands, their spectral strengths are sensitively dependent on the pump intensity. Varying pump power, one can change their spectral strengths significantly.[9]

Subsideband generation is observed in the laser when the strength of a sideband has become strong enough. Figure 1(b) shows one form of the experimentally observed subsidebands. Figure 1(b) shows that as a sideband becomes unstable, two new discrete spectral components simultaneously appear on each side of it. The newly generated subsidebands have relatively large wavelength shifts in relation to the unstable sideband (of the magnitude of several nanometers). Occasionally, higher-order subsidebands are also observed. Once the strongest sideband becomes unstable, normally subsidebands with different wavelength shifts also appear on the other lower-intensity sidebands, which we attribute to cross coupling between the subsidebands in the laser.

The formation of this form of subsidebands exists only in a very narrow pump range. As the pump power is further increased, new soliton pulses form in the cavity. Consequently the strengths of all sidebands suddenly drop, and the subsidebands disappear. However, as the pump power is continuously increased, the same procedure repeats.[13]

Figure 1(c) shows another form of the subsideband generations observed. Compared with the subsidebands shown in Fig. 1(b), these subsidebands have significantly smaller wavelength shifts, which in our experiments are less than 1 nm. This subsideband generation can exist in a large pump-power range. Higher orders of the subsidebands are always observed. They appear one by one as the pump power is increased. Figure 2 shows as an example the evolution of the subsidebands with the pump power. Initially a sideband has weak spectral strength, and its spectrum has a single peak. As the pump power

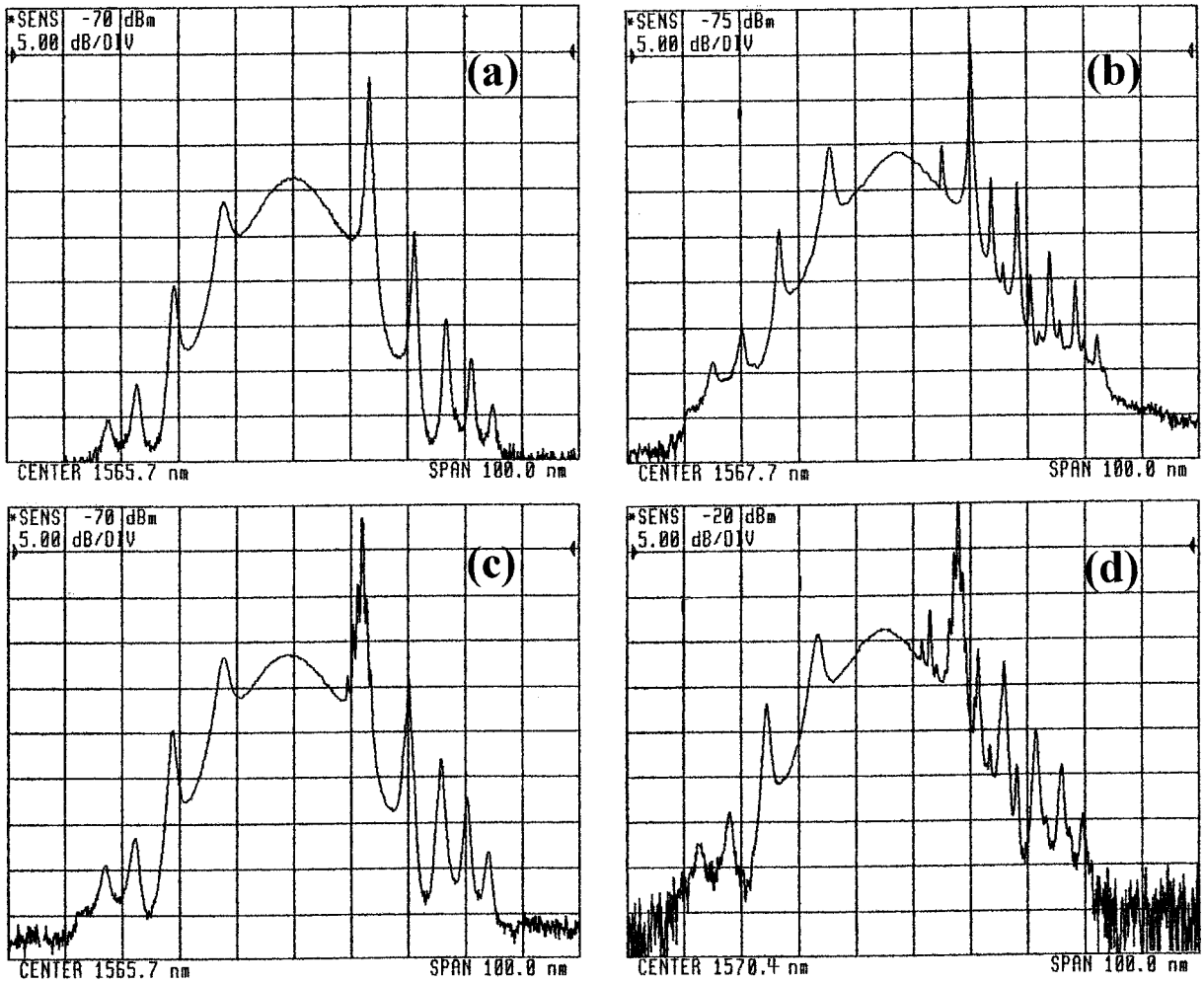

Fig. 1. Experimentally measured soliton spectra of the laser: (a) soliton spectrum without subsideband generation; (b) soliton spectrum with large wavelength-shifted subsidebands; (c) soliton spectrum with small wavelength-shifted subsidebands; (d) soliton spectrum with coexistence of the two subsidebands.

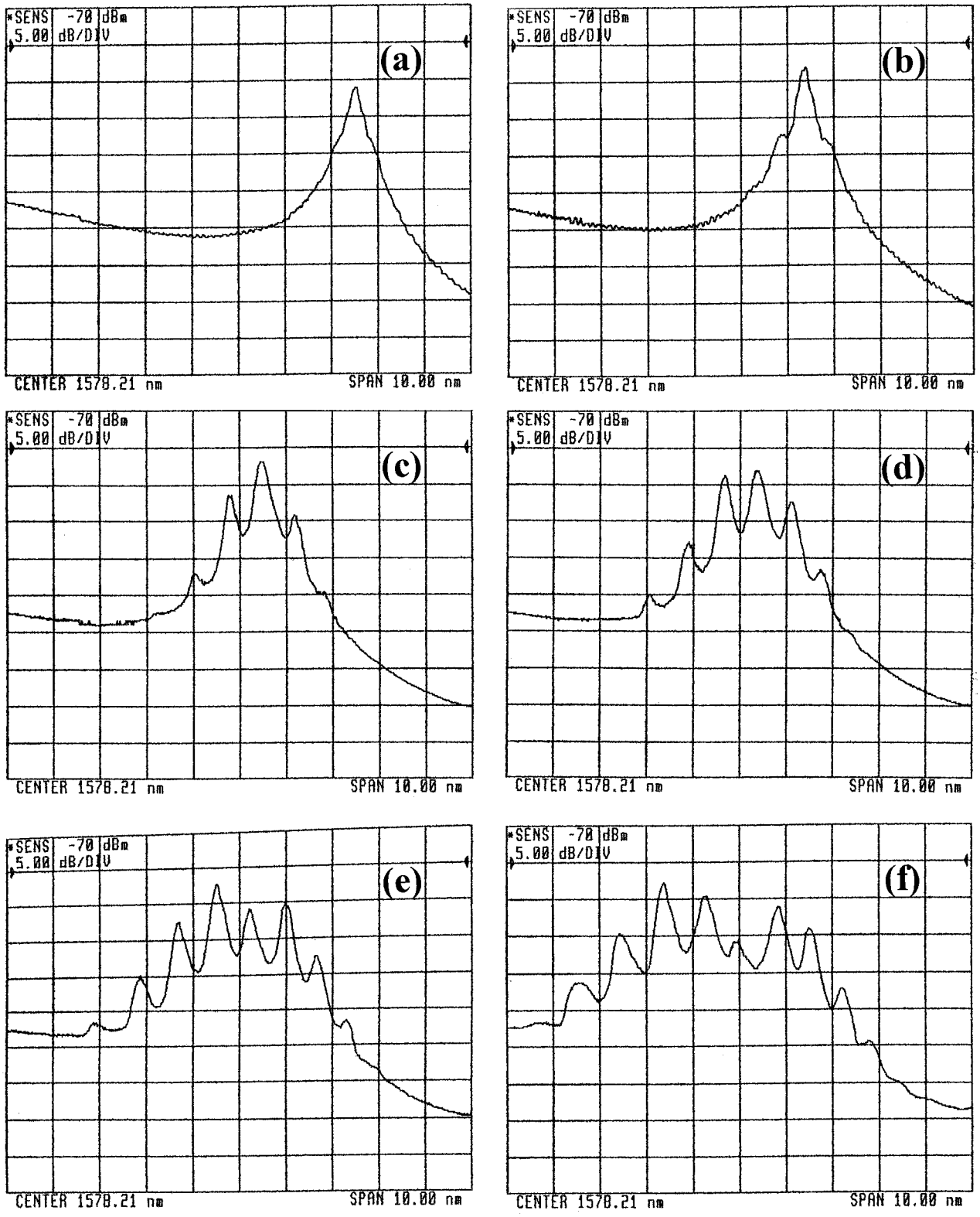

Fig. 2. Evolution of the small wavelength-shifted subsidebands with the pump power. From (a) to (f), only the pump power is increased; other laser parameters are fixed: (a) 80 mW, (b) 98 mW, (c) 114 mW, (d) 122 mW, (e) 130 mW, and (f) 133 mW. The reference levels of the spectra are the same.

is increased, the strength of the sideband increases, and eventually it becomes unstable. Two small wavelength-shifted subsidebands appear on each side of it.

With a further increase in the pump power, higher-order subsidebands appear. Obviously the wavelength shifts of the subsidebands with respect to the unstable sideband are pump-power dependent. When several higher-order subsidebands appear, the spectral strength of the unstable sideband can also become weaker than those of the subsidebands as shown in Figs. 2(e) and 2(f),

showing strong sideband depletion. With a continuous increase in the pump power, new soliton pulses eventually form in the laser cavity, the strength of the sideband suddenly drops, and all the subsidebands disappear. Exactly the same procedure as observed in the other form of subsideband generation takes place.

We experimentally investigated conditions in which each of these subsidebands appears. We found that with an appropriate experimental parameter setting, one can switch the subsideband generation from one form to the other, simply by rotating one of the quarter-wave plates in the polarization controller before the isolator. Physically, this has an effect of changing the linear phase bias of the nonlinear polarization rotation, which in our case of mode locking is equivalent to changing the strength of the saturable-absorption effect of the laser. By carefully setting the saturable-absorption strength, we also observed the coexistence of both forms of the subsideband, as shown in Fig. 1(d). Under this coexistence, further complicated discrete spectral components appear, which could again be attributed to cross coupling between the subsidebands.

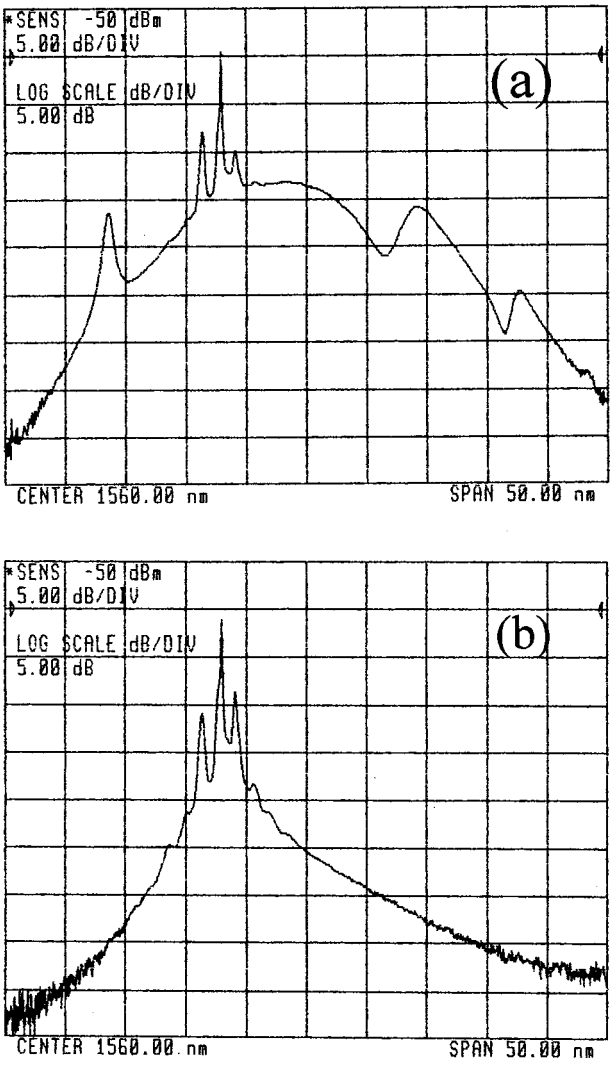

Fig. 3. cw Mode excitation in the fiber soliton laser: (a) soliton spectrum with cw mode excitation; (b) steady-state lasing spectrum. From (a) to (b), only the pump power is reduced to below the soliton-operation threshold; other laser parameters are fixed.

Spurious spectral component generation in the soliton spectrum of fiber soliton lasers has frequently been observed experimentally.[14,15] The most general cases are the excitation of cw laser modes. In our experiment we also observed such cw mode excitation. However, we found that cw mode excitation can easily be identified experimentally. As an example, we show one of these cases in Fig. 3. Figure 3(a) shows a soliton spectrum with three discrete spectral components appearing in it. Figure 3(b) shows the corresponding cw lasing spectrum obtained by reducing the pump power to below the soliton-operation threshold while fixing all other laser parameters. Comparing the spectra, it becomes clear that the discrete spectral components are the cw mode excitation, as they have exactly the same spectral positions in Figs. 3(a) and 3(b). Other features of cw mode excitation, such as the dependence of the excited mode on the minimum cavity-loss position, can also be used to identify it.

3. NUMERICAL SIMULATIONS

To analyze our experimental observations, we also conducted numerical simulations to study the subsideband generation in the laser. Passively mode-locked fiber soliton lasers have been theoretically investigated intensively in the past.[16–19] However, the majority of studies have concentrated on the master-equation model. Although the master equation has already given a very good description of laser operation, such as the mode-locking mechanism and soliton formation, a fundamental limitation of the model is that it is built up under the assumption that the nonlinear pulse change over one round trip is small. In the reality of a fiber soliton laser this condition is obviously not always fulfilled. In particular, the dispersive wave effects and the polarization effects of light circulating in a birefringent cavity are not included in the master equation, which could also play an important role in the laser dynamics. To take all these effects into consideration, we conducted our numerical simulations with a different approach. Specifically, we describe the soliton propagation in the fiber with the coupled nonlinear Schrödinger equations of the form[20,21]

$$\frac{\partial u}{\partial z} = i\beta v - \delta\frac{\partial v}{\partial t} + \frac{i}{2}\beta''\frac{\partial^2 u}{\partial t^2} + i2\gamma \times \left(\frac{1}{3}|u|^2 u + \frac{2}{3}|v|^2 u\right) + \frac{g}{2}u, \tag{1a}$$

$$\frac{\partial v}{\partial z} = i\beta u - \delta\frac{\partial u}{\partial t} + \frac{i}{2}\beta''\frac{\partial^2 v}{\partial t^2} + i2\gamma \times \left(\frac{1}{3}|v|^2 v + \frac{2}{3}|u|^2 v\right) + \frac{g}{2}v, \tag{1b}$$

where u and v are the normalized envelopes of the optical pulses along the two circularly polarized modes of the

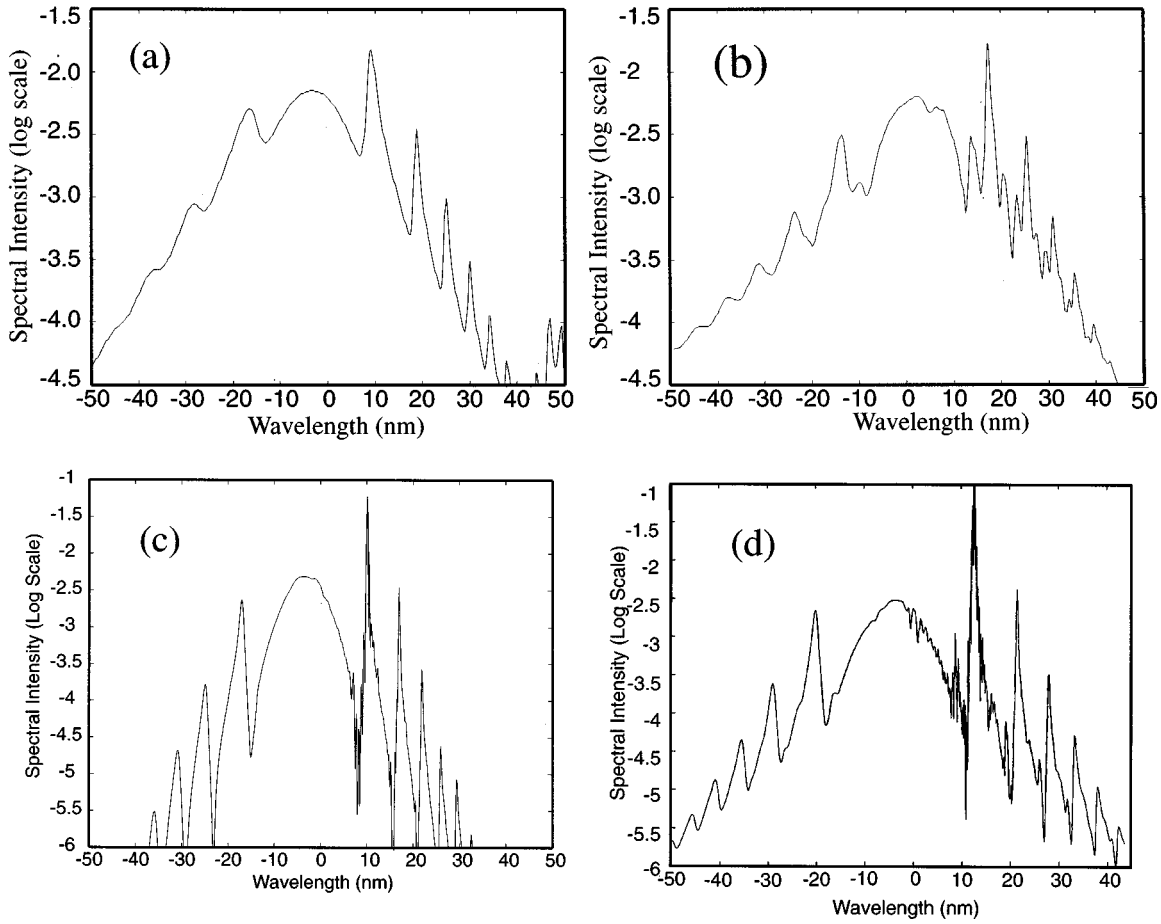

Fig. 4. Soliton spectra calculated numerically: (a) soliton spectrum without subsidebands ($g_p = 1300$, phase bias of $\pi/3$); (b) soliton spectrum with strong saturable absorption ($g_p = 1400$, phase bias of $\pi/3$); (c) soliton spectrum with weak saturable absorption ($g_p = 600$, phase bias of $2\pi/3$); (d) soliton spectrum with moderate saturable absorption ($g_p = 800$, phase bias of $\pi/1.7$). Other parameters used are $\Omega g = 2\pi * 10$ THz, $\gamma = 3\ \mathrm{W^{-1}\,km^{-1}}$, $\beta_1'' = -2$ (ps/nm)km, $\beta_2'' = -10$ (ps/nm)km, cavity length $L = 12$ m, and beat length $L_b = L/5$.

fiber. We note that in order to take into account the wave-mixing effect and for the sake of easy numerical calculation, we transformed the coupled nonlinear Schrödinger equations into the form of two circularly polarized fiber modes. $2\beta = 2\pi\Delta n/\lambda$ is the wave-number difference between the modes (π/β is the fiber's beat length). $2\delta = 2\beta\lambda/2\pi c$ is the inverse group-velocity difference. β'' is the second-order dispersion, and γ is the nonlinearity of the fiber. g is the saturable gain of the erbium-doped fiber. For undoped fiber, $g = 0$. The gain dispersion of the fiber is approximated by

$$g(\omega) = g_p\left[1 - \left(\frac{\omega - \omega_0}{\Omega_g}\right)^2\right], \tag{2}$$

where g_p is the peak gain, ω_0 is the peak-gain frequency position, and Ω_g is the gain bandwidth. The coupled equations (1a) and (1b) are numerically solved with the standard split-step method. We simulate the laser cavity effect by circulating the light in the cavity and describe the actions of the isolator and polarization controllers on the soliton pulses with their transformation matrices. With this approach the nonlinear self-amplitude modulation effect and the cavity-loss dispersion effect are automatically included in the simulation. In all our calculations a noise light pulse is initially used as the input. We let it circulate in the cavity; after one round trip, we then use the final state as the input for the next round trip, until a stable steady state or a quasi steady state is reached. We then compare the steady-state pulse parameters with our experimental results.

Where it is possible, we used parameters corresponding to the experimental conditions for our simulations. Figure 4 shows results of the numerical simulations. Figure 4(a) shows the soliton spectrum obtained with weak pump power. As expected, the soliton spectrum has no subsidebands. We emphasize that Fig. 4(a) has all the characteristics of those observed experimentally. In particular, the strengths of the sidebands exhibit strong asymmetry. With an increase in pump power, the strengths of the sidebands increase. To a certain level, discrete subsidebands appear in the soliton spectrum, as shown in Fig. 4(b). These subsidebands have large wavelength shifts in relation to the unstable sideband. Subsidebands caused by the cross coupling are also visible in the spectrum and are in good agreement with the experimental result shown in Fig. 1(b). We then reduced the saturable-absorber effect in the simulation while fixing

all other parameters. This is done by a change in the phase bias in the mode locking. Figure 4(c) shows the result obtained. With reduced saturable absorption the small wavelength-shifted subsidebands appear, which confirms our experimental observations that the different forms of the subsideband generation are determined by the different strength of the saturable-absorber effect in the laser cavity. Figure 4(d) shows that with a saturable-absorption strength between those of Figs. 4(b) and 4(c), both forms of subsideband generation occur simultaneously, which again corresponds to the experimental result shown in Fig. 1(d).

4. DISCUSSION

Before we explain results of our experimental and numerical observations, we first note that we have studied features of the subsideband generation with large wavelength shifts.[22] We have identified its physical origin as being the modulational instability in the laser. The large wavelength shifts of the subsidebands are a result of the influence of the periodic dispersion variation on the classic modulational instability. In our fiber laser, because the erbium-doped fiber and the dispersion-shifted fibers used have different dispersions, light circulating in the cavity experiences periodic dispersion variations. As demonstrated theoretically and numerically by other authors,[23–25] this periodic dispersion variation changes the gain structure of the classic modulational instability and introduces large wavelength-shifted gain.

Studying the features of the small wavelength-shifted subsidebands, we identified that their physical origin is again the modulation instability. As evidenced in Fig. 2, the appearance of the subsidebands is a threshold effect and is dependent on the strength of the sideband. The subsidebands always appear in a Stokes and anti-Stokes pair in the soliton spectrum, which indicates that their appearance is a parametric process. The wavelength shifts of the subsidebands vary with the pump power, which is again a typical characteristic of modulational instability. To further demonstrate the power-tuning characteristic of the subsidebands, we show in Fig. 5 the experimentally measured wavelength shifts of all subsidebands with the pump power.

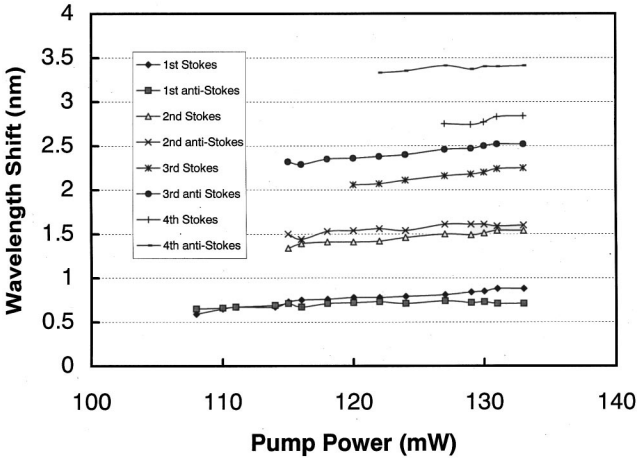

Fig. 5. Power-tuning characteristics of the small wavelength-shifted subsidebands. Wavelength shifts are measured in relation to the unstable sideband.

Both forms of the subsideband generation are therefore caused by modulational instability. Based on this, the relation between the generation of different forms of the subsidebands and the strength of the saturable absorption becomes clear. From the numerical simulation of periodic dispersion variation on the classic modulational instability gain,[23–25] it is easy to see that the modified gain actually includes both small and large wavelength-shifted gains. Without the existence of the saturable-absorber effect one would expect that the small wavelength-shifted subsidebands would appear first, as they have relatively larger gain. And depending on the pump power, the larger wavelength-shifted subsidebands would gradually appear. However, the existence of a saturable absorber in the laser cavity could change the effective gain distribution. A saturable absorber has the effect that it suppresses low power variations but favors high power variations. In the case of modulational instabilities, a larger wavelength-shifted subsideband corresponds to a quicker power variation and has higher peak power. It will therefore experience less loss caused by the saturable absorber. In contrast a lower wavelength-shifted subsideband will experience stronger loss. So depending on the relative strength between the saturable-absorber effect and the modulational-instability gain, different outcomes could appear, as demonstrated in our experiments.

However, we point out that the observed subsidebands in both cases have asymmetric wavelength shifts, which is different from those observed in the modulational instability in optical fibers, where in contrast the Stokes and the anti-Stokes spectral components have exactly the same wavelength shifts.[26,27] To explain this difference, we emphasize that the subsidebands observed in our experiment are in fact results of modulational-instability lasing.[28,29] This is different from the modulational instabilities in optical fibers, where the instability spectral lines are generated at the modulational-instability gain peaks, which therefore have exactly the same wavelength shifts. In the case of modulational-instability lasing the spectral positions of the subsidebands are determined not only by the modulational-instability gain peak positions but also by the cavity-mode position and the cavity-dispersion properties. As in a fiber soliton laser, strong cavity dispersion exists, which results in asymmetry in Stokes and anti-Stokes wavelength shifts of the subsidebands. We note that the experimentally observed asymmetry of the wavelength shifts in both forms of the subsideband generation are dependent on the magnitude of the wavelength shift: the larger the wavelength shift, the stronger the asymmetry. Also within the experimental error range, both forms of the subsideband generation have the same characteristic of asymmetric wavelength shifts: namely, the anti-Stokes components always have larger wavelength shifts than the Stokes components do. All these observed features are in good agreement with our analysis and are reproduced in the numerical simulations.

Finally, we point out that subsideband generation has been observed to occur only to the sidebands, rather than to the cw mode spectrum, even when the spectral inten-

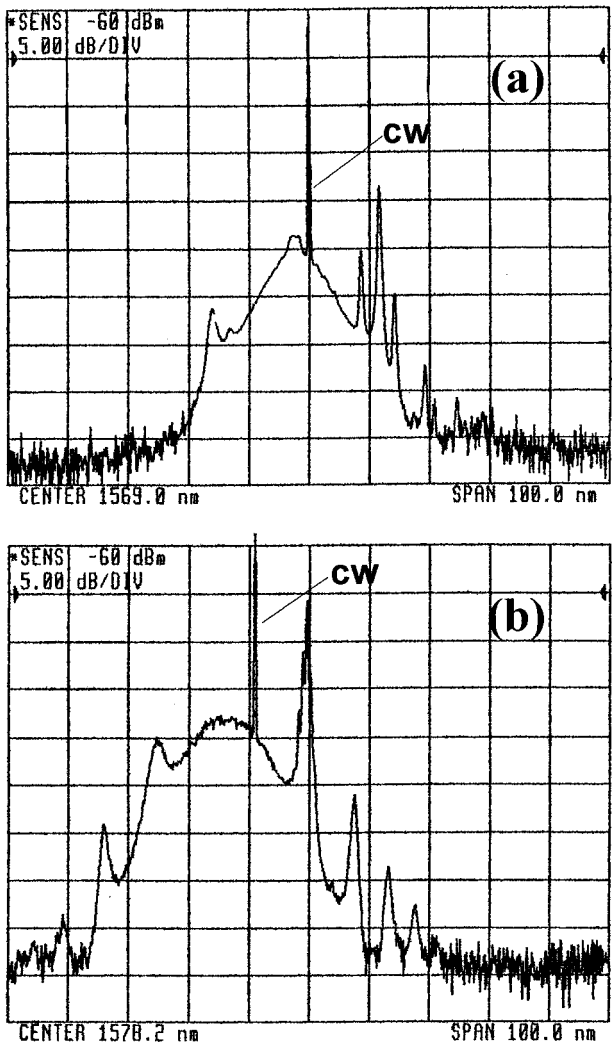

Fig. 6. Soliton spectra with coexistence of cw mode excitation and subsideband generation: (a) a case with large wavelength-shifted subsidebands; (b) a case with small wavelength-shifted subsidebands.

sity of the latter is far stronger than that of an unstable sideband, as shown in Fig. 6. This experimental result strongly supports the point of view that the dispersive waves in a fiber soliton laser are long-duration pulses, rather than cw as has been pointed out by several other authors.[30] As the dispersive waves are pulsed, their peak power could be very high. Despite the fact that dispersive waves are generally very weak, modulational instability could still occur in them. In the case of a fiber laser the cavity-resonance effect and the cavity gain can further reduce the modulational-instability threshold and can lead to the observation of the phenomenon.[31]

5. CONCLUSIONS

In conclusion, we have experimentally observed two forms of subsideband generation in an ultrashort-pulse fiber soliton laser. We found that the different forms of the subsideband generation are related to the different strengths of the saturable absorption in the laser. In particular, with strong saturable absorption, the larger wavelength-shifted subsidebands are observed, whereas with weak saturable absorption, the small wavelength-shifted subsidebands are observed. Studying characteristics of the subsideband generation, we identified that they are both results of the modulational-instability lasing of the dispersive waves in the laser. Numerical simulations confirm our experimental results.

REFERENCES

1. D. J. Richardson, R. I. Laming, D. N. Payne, V. I. Matsas, and M. W. Phillips, "Pulse repetition rates in passive, self-starting, femtosecond soliton fiber laser," Electron. Lett. **27**, 1451–1453 (1991).
2. M. Nakazawa, E. Yoshida, and Y. Kimiura, "Low threshold, 290fs erbium-doped fiber laser with a nonlinear amplifying loop mirror pumped by InGaAsP laser diodes," Appl. Phys. Lett. **59**, 2073–2075 (1991).
3. R. P. Davey, N. Langford, and A. I. Ferguson, "Interacting solitons in erbium fiber laser," Electron. Lett. **27**, 1257–1259 (1991).
4. M. L. Dennis and I. N. Duling III, "Experimental study of sideband generation in femtosecond fiber lasers," IEEE J. Quantum Electron. **30**, 1469–1477 (1994).
5. S. M. J. Kelly, "Characteristic sideband instability of periodically amplified average soliton," Electron. Lett. **28**, 806–807 (1992).
6. D. U. Noske, N. Pandit, and J. R. Taylor, "Source of spectral and temporal instability in soliton fiber lasers," Opt. Lett. **17**, 1515–1517 (1992).
7. N. J. Smith, K. J. Blow, and I. Andonovic, "Sideband generation through perturbations to the average soliton model," J. Lightwave Technol. **10**, 1329–1333 (1992).
8. N. Pandit, D. U. Noske, S. M. J. Kelly, and J. R. Taylor, "Characteristic instability of fiber loop soliton lasers," Electron. Lett. **28**, 455–457 (1992).
9. D. Y. Tang, P. D. Drummond, W. S. Man, and H. Y. Tam, "Observation of modulation instability in a fiber soliton ring laser," Opt. Commun. **167**, 125–128 (1999).
10. M. Hofer, M. E. Fermann, F. Haberl, M. H. Ober, and A. J. Schmidt, "Mode locking with cross-phase and self-phase modulation," Opt. Lett. **16**, 502–504 (1991).
11. K. Tamura, H. A. Haus, and E. P. Ippen, "Self-starting additive pulse mode-locked erbium fiber ring laser," Electron. Lett. **288**, 2226–2228 (1992).
12. W. S. Man, H. Y. Tam, M. S. Demokan, P. K. A. Wai, and D. Y. Tang, "Mechanism of intrinsic wavelength tuning and sideband asymmetry in a passively mode-locked soliton fiber ring laser," J. Opt. Soc. Am. B **17**, 28–33 (2000).
13. D. Y. Tang, W. S. Man, and H. Y. Tam, "Stimulated soliton pulse generation in a passively mode locked fiber soliton laser," Opt. Commun. **165**, 189–194 (1999).
14. M. J. Guy, D. U. Noske, and J. R. Taylor, "Generation of femtosecond soliton pulses by passive mode locking of an ytterbium-erbium figure-of-eight fiber laser," Opt. Lett. **18**, 1447–1449 (1993).
15. S. Namiki, E. P. Ippen, H. A. Haus, and K. Tamura, "Relaxation oscillation behavior in polarization additive pulse mode-locked fiber ring lasers," Appl. Phys. Lett. **69**, 3969–3971 (1996).
16. H. A. Haus, E. P. Ippen, and K. Tamura, "Additive-pulse modelocking in fiber lasers," IEEE J. Quantum Electron. **30**, 200–207 (1994).
17. H. A. Haus, J. G. Fujimoto, and E. P. Ippen, "Analytic theory of additive pulse and Kerr lens mode locking," IEEE J. Quantum Electron. **28**, 2086–2096 (1992).
18. H. A. Haus, J. G. Fujimoto, and E. P. Ippen, "Structures for additive pulse mode locking," J. Opt. Soc. Am. B **8**, 2068–2076 (1991).
19. C. J. Chen, P. K. A. Wai, and C. R. Menyuk, "Soliton fiber ring laser," Opt. Lett. **17**, 417–419 (1992).
20. C. R. Menyuk, "Nonlinear pulse propagation in birefringent optical fibers," IEEE J. Quantum Electron. **23**, 174–176 (1987).
21. S. G. Evangelides, Jr., L. F. Mollenauer, J. P. Gordon, and

N. S. Bergans, "Polarization multiplexing with solitons," J. Lightwave Technol. **10**, 28–35 (1992).
22. D. Y. Tang, W. S. Man, H. Y. Tam, and M. S. Demokan, "Modulational instability in a fiber soliton ring laser induced by periodic dispersion variation," Phys. Rev. A **61**, 023804 (2000).
23. N. J. Smith and N. J. Doran, "Modulational instabilities in fibers with periodic dispersion management," Opt. Lett. **21**, 570–572 (1996).
24. F. Kh. Abdullaev and J. Garnier, "Modulational instability of electromagnetic waves in birefringent fibers with periodic and random dispersion," Phys. Rev. E **60**, 1042–1050 (1999).
25. J. C. Bronski and J. N. Kutz, "Modulational stability of plane waves in nonreturn-to-zero communications systems with dispersion management," Opt. Lett. **21**, 937–939 (1996).
26. K. Tai, A. Hasegawa, and A. Tomita, "Observation of modulational instability in optical fibers," Phys. Rev. Lett. **56**, 135–138 (1986).
27. F. Ito, K. Kitayama, and H. Yoshinaga, "Experimental verification of frequency level-off of modulational instability in the minimum dispersion region," Appl. Phys. **54**, 2503–2505 (1989).
28. P. Franco, F. Fontana, I. Cristiani, M. Midrio, and M. Romagnoli, "Self-induced modulation instability laser," Opt. Lett. 2009–2011 (1995).
29. E. Yoshida and M. Nakazawa, "Low-threshold 115-GHz continuous-wave modulational instability erbium-doped fiber laser," Opt. Lett. **22**, 1409–1411 (1997).
30. A. B. Grudinin and S. Gray, "Passive harmonic modelocking in soliton fiber lasers," J. Opt. Soc. Am. B **14**, 144–154 (1997).
31. G. P. Agrawal, "Modulation instability in erbium-doped fiber amplifiers," IEEE Photon. Technol. Lett. **4**, 562–564 (1992).